

AperTO - Archivio Istituzionale Open Access dell'Università di Torino

PT-symmetrically deformed shock waves

This is a pre print version of the following article:

Original Citation:

Availability:

This version is available <http://hdl.handle.net/2318/1871901> since 2022-08-09T11:13:43Z

Terms of use:

Open Access

Anyone can freely access the full text of works made available as "Open Access". Works made available under a Creative Commons license can be used according to the terms and conditions of said license. Use of all other works requires consent of the right holder (author or publisher) if not exempted from copyright protection by the applicable law.

(Article begins on next page)

\mathcal{PT} -symmetrically deformed shock waves

Andrea Cavaglia and Andreas Fring

*Centre for Mathematical Science, City University London,
Northampton Square, London EC1V 0HB, UK
E-mail: andrea.cavaglia.1@city.ac.uk, a.fring@city.ac.uk*

ABSTRACT: We investigate for a large class of nonlinear wave equations, which allow for shock wave formations, how these solutions behave when they are \mathcal{PT} -symmetrically deformed. For real solutions we find that they are transformed into peaked solutions with a discontinuity in the first derivative instead. The systems we investigate include the \mathcal{PT} -symmetrically deformed inviscid Burgers equation recently studied by Bender and Feinberg, for which we show that it does not develop any shocks, but peaks instead. In this case we exploit the rare fact that the \mathcal{PT} -deformation can be provided by an explicit map found by Curtright and Fairlie together with the property that the undeformed equation can be solved by the method of characteristics. We generalise the map and observe this type of behaviour for all integer values of the deformation parameter ε . The peaks are formed as a result of mapping the multi-valued self-avoiding shock profile to a multi-valued self-crossing function by means of the \mathcal{PT} -deformation. For some deformation parameters we also investigate the deformation of complex solutions and demonstrate that in this case the deformation mechanism leads to discontinuities.

1. Introduction

Since the proposal that complex \mathcal{PT} -symmetric quantum mechanical Hamiltonians may be viewed as self-consistent descriptions of physical systems [1], \mathcal{PT} -symmetry has been exploited to propose and study many more complex extensions of real systems. Numerous new quantum mechanical and quantum field theoretical models have been investigated, see for instance [2, 3, 4] for recent reviews. Inspired by this success, the construction principle has also been used to suggest new classical models, such as complex extensions of standard one particle real quantum mechanical potentials [5, 6, 7, 8, 9, 10], non-Hamiltonian dynamical systems [11], chaotic systems [12] and deformations of many-particle systems such as Calogero-Moser-Sutherland models [13, 14, 15, 16, 17, 18, 19]. Here we will mainly focus on extensions of nonlinear wave type, such as the prototype Korteweg-deVries (KdV) equation [20, 21, 22] and closely related models [23, 24, 25, 26, 27]. In [27] it was demonstrated that when reduced these systems can also shed light on large classes of one particle quantum mechanical models.

As is well known from transformation theory a lot of new information on nonlinear wave equations can be obtained from transformed equations by means of for instance Hopf-Cole, Miura or Bäcklund type. In a somewhat similar spirit we also exploit here the knowledge of a transformation in form of an explicitly known \mathcal{PT} -symmetrical deformation. Here we will mainly focus on the question of what kind of effect a \mathcal{PT} -deformation has on a shock wave. It is well known that a shock forms when the crest of a wave overtakes the troughs. The challenge for a mathematical description is that one can no longer describe this phenomenon by a function since the surface of the wave becomes multi-valued. For real wave equations solvable with the method of characteristics, this happens when two characteristics cross each other or more generally when the first derivative becomes infinite. For \mathcal{PT} -deformed equations remaining real, we argue here that the first derivative is discontinuous but remains finite, whereas the second derivative tends to infinity. Solitonic solutions with this type of behaviour are often referred to as peakons [28]. When the deformation parameters are non odd integers, one is forced to consider complex solutions even in the undeformed case if one demands a real solution for the deformed one. However, evolving this real deformed solution in time will convert it into a complex one. In addition, when compared to the real scenario, the peaks vanish and we observe discontinuities, which are generated due to the imposition of physical asymptotic boundary conditions.

Our manuscript is organised as follows: In section 2 we describe the \mathcal{PT} -deformed models we are investigating and how the explicit knowledge of the deformation map can be utilised to extract information about the systems, in particular the shock time and conservation laws. In section 3 we describe the general mechanism of how real shock waves are mapped into peaks and in section 4 how a modification of this mechanism leads to jumps in a complex scenario. In section 5 we present various numerical case studies supporting and illustrating our findings. We present our conclusions in section 6.

2. Shock times and conservations laws from \mathcal{PT} -deformation maps

The model we wish to study here with regard to shock wave and peak formation is a \mathcal{PT} -symmetrical deformation of a nonlinear wave equation

$$\mathcal{PT}_\varepsilon : \quad w_t + f(w)w_x = 0 \quad \rightarrow \quad u_t - if(u)(iu_x)^\varepsilon = 0, \quad (2.1)$$

with $f(w)$ being a well behaved function of w . Clearly the undeformed equation is \mathcal{PT} -symmetric, that is being invariant under a simultaneous reflection in time $t \rightarrow -t$ and space $x \rightarrow -x$, when $\mathcal{PT} : f(w) \rightarrow f(w)$, $w \rightarrow cw$ with $c \in \mathbb{C}$. The deformed equation is constructed as usual by taking into account that the \mathcal{PT} -transformation is antilinear [29] and an overall minus sign in the second term is generated from $i \rightarrow -i$ rather than from $x \rightarrow -x$. The special case $f(w) = w$ corresponds to the \mathcal{PT} -symmetrical deformation of the inviscid Burgers equation, also referred to as Riemann-Hopf or Euler-Monge equation, recently studied by Bender, Feinberg [23] and Curtright, Fairlie [24]. The real version of the first equation in (2.1), especially for $f(w) = w$, appears mainly in fluid mechanics whereas its complex version is frequently encountered in the treatment of large N matrix models, see e.g. [30].

Most wave equations are only directly related to their \mathcal{PT} -symmetric deformations in the limit $\varepsilon \rightarrow 1$ and an explicit transformation between the two is not known otherwise. For instance, this is the case for the deformations of the KdV-equation [20, 21, 22, 27]. In contrast, in some rare cases the deformation map \mathcal{PT}_ε constitutes an explicit transformation from the undeformed to the deformed system. As pointed out by Curtright and Fairlie [24] for the system (2.1) with $f(w) = w$, the first equation in (2.1) converts into the second under the map $w \mapsto \varepsilon u(iu_x)^{\varepsilon-1}$. We generalise this here to equations with arbitrary $f(w)$ to

$$\begin{aligned} \mathcal{PT}'_\varepsilon : \quad w &\mapsto \varepsilon f(u)(iu_x)^{\varepsilon-1}, \\ w_t + ww_x &= 0 \quad \rightarrow \quad u_t - if(u)(iu_x)^\varepsilon = 0. \end{aligned} \quad (2.2)$$

This is seen as follows: Defining $u = g(v)$ it is easy to verify that the deformed equation in (2.1) is converted into the deformed inviscid Burgers equation for v

$$v_t - iv(iv_x)^\varepsilon = 0, \quad (2.3)$$

provided the constraint

$$v = f[g(v)][g'(v)]^{\varepsilon-1} \quad (2.4)$$

holds. Since we know already that $w \mapsto \varepsilon v(iv_x)^{\varepsilon-1}$ maps the inviscid Burgers equation to the deformation (2.3), we can derive from this the general map (2.2) when using (2.4) and $v_x = u_x/g'(v)$. Note that the explicit form for the function $g(v)$ is only required when we want to discuss equation (2.3) in relation to the equation involving u . Essential is here only its existence, which follows from the fact that (2.4) is separable.

Instead of $\mathcal{PT}'_\varepsilon$, which transforms the inviscid Burgers equation, we can also construct \mathcal{PT}_ε , although in that case we have to be more specific about $f(w)$. Taking for instance $f(w) = w^n$ the first equation in (2.1) converts into the second under the map

$$\mathcal{PT}_\varepsilon : \quad w \mapsto \sqrt[n]{\varepsilon u(iu_x)^{\varepsilon-1}}. \quad (2.5)$$

Apart from the i , for $n = 1$ this reduces to the map found by Curtright and Fairlie [24].

These explicit maps (2.2) and (2.5) can now be exploited to investigate properties of the deformed equations. We start by considering in more detail how the solutions of the w -equation in (2.1) are mapped into solutions of the deformed system. It is well known that the undeformed equation can be solved by the method of characteristics. The characteristic, i.e. the curve in the xt -plane at which $w(x, t) = w(x_0, 0) =: w_0(x_0)$ is conserved, acquires in that case the form

$$x = f(w_0)t + x_0. \quad (2.6)$$

The gradient catastrophe occurs when two of these characteristics cross or equivalently when w_x tends to infinity. Considering therefore

$$w_x = w'_0(x_0) \frac{dx_0}{dx} = \frac{w'_0(x_0)}{1 + t \frac{df(w_0)}{dx_0}}, \quad (2.7)$$

we can read off the earliest time, that is the breaking or shock time t_s^w , and the corresponding position x_s^w from (2.6) for which this happens

$$t_s^w = \min \left(-1 / \frac{df(w_0)}{dx_0} \right) > 0 \quad \text{and} \quad x_s^w = f[w_0(x_0^{\min})] t_s^w + x_0^{\min}. \quad (2.8)$$

Our concern here is how this translates into the deformed set of equations, i.e. what are the corresponding times t_s^u and positions x_s^u and moreover do the deformed systems exhibit shocks?

When $f(w) = w^n$ the shock time resulting from (2.8) is

$$t_s^w = - \frac{1}{\sqrt[n]{\varepsilon} \frac{d}{dx_0} \left[\sqrt[n]{u_0} (i u_{x_0})^{\frac{\varepsilon-1}{n}} \right]}. \quad (2.9)$$

For $n = 1$ the expression (2.9) agrees precisely with the formula (22) in [23], derived by analysing directly the deformed equation in (2.1) with the more complicated method of characteristic strips. Clearly we need to demand that the time is real, which is guaranteed when we replace $u_0 \rightarrow i^\alpha \hat{u}_0$ with $\hat{u}_0 \in \mathbb{R}$ and $\alpha = (4m \pm 1)n/\varepsilon$, $m \in \mathbb{Z}$. Thus for certain combinations of ε and n we loose the possibility of shock wave generation for real solutions of the deformed equation. Nonetheless, in these cases we have a correspondence between a real undeformed solution and a complex deformed one. However, we will demonstrate in section 4 that if we do not insist in the undeformed solution to be real a shock formation is indeed possible, in constrast to the claims in [23].

Other quantities of interest which may be obtained from the explicit \mathcal{PT} -maps are conserved quantities. A conservation law for the first equation in (2.1) is simply derived by multiplying it with $\kappa f(w)^\kappa$ and subsequent re-arrangement

$$[f(w)^\kappa]_t + \frac{\kappa}{\kappa+1} [f(w)^{\kappa+1}]_x = 0. \quad (2.10)$$

Therefore for any asymptotically vanishing function $f(w)$ and constant $\kappa \in \mathbb{R} \setminus \{-1\}$ the quantities

$$I_\kappa(w) = \int_{-\infty}^{\infty} f[w(x,t)]^\kappa dx, \quad (2.11)$$

are conserved in time. Correspondingly, we find for the deformed system the transformed charges

$$I_\kappa(u) = \int_{-\infty}^{\infty} f[\varepsilon f(u) (i u_x)^{\varepsilon-1}]^\kappa dx. \quad (2.12)$$

We will make use of these conserved quantities below.

3. Peak formation mechanisms from real shock waves

Having confirmed the result for the expression of the shock times by Bender and Feinberg in an alternative simpler manner, we deviate, however, from their interpretation of this result. Unlike Bender and Feinberg we conclude that these times correspond in general not to a gradient but rather to a curvature catastrophe, i.e. the first derivative stays finite

whereas the second tends to infinity. We reason as follows: For $n = 1$ it follows obviously from (2.5) that

$$w_x = i\varepsilon(iu_x)^{\varepsilon-2} [u_x^2 + (\varepsilon - 1)uu_{xx}]. \quad (3.1)$$

This means that a possible shock in the \mathcal{PT} -symmetrically deformed inviscid Burgers equation, $u_x \rightarrow \infty$, would always correspond to a shock in the undeformed equation, that is $w_x \rightarrow \infty$. However, the reverse does not necessarily follow as a shock in the undeformed equation might correspond to $u_{xx} \rightarrow \infty$ with finite u_x , rather than to $u_x \rightarrow \infty$. Thus in the former scenario the shock time for the undeformed equation in (2.1) would correspond to a formation time of a different type of wave profile in the deformed equation in (2.1). We can identify the explicit form by expressing u in terms of w and use these expressions for our analysis. We find

$$u(x, t) = (-i)^{1-\frac{1}{\varepsilon}} (\varepsilon - 1)^{\frac{1}{\varepsilon}-1} \varepsilon^{\frac{\varepsilon-2}{\varepsilon}} \left[\int^x w(q, t)^{\frac{1}{\varepsilon-1}} dq \right]^{\frac{\varepsilon-1}{\varepsilon}}. \quad (3.2)$$

Differentiating this twice we obtain

$$u_x(x, t) = (-i)^{1-\frac{1}{\varepsilon}} (\varepsilon - 1)^{\frac{1}{\varepsilon}} \varepsilon^{-\frac{2}{\varepsilon}} w(x, t)^{\frac{1}{\varepsilon-1}} \left[\int^x w(q, t)^{\frac{1}{\varepsilon-1}} dq \right]^{-\frac{1}{\varepsilon}}, \quad (3.3)$$

$$\begin{aligned} u_{xx}(x, t) &= (-i)^{1-\frac{1}{\varepsilon}} (\varepsilon - 1)^{\frac{1}{\varepsilon}-1} \varepsilon^{\frac{\varepsilon-2}{\varepsilon}} \left(\int^x w(q, t)^{\frac{1}{\varepsilon-1}} dq \right)^{-\frac{\varepsilon+1}{\varepsilon}} w(x, t)^{\frac{2}{\varepsilon-1}} \\ &\quad \times \left[\varepsilon \left(1 - \varepsilon + \int^x w(q, t)^{\frac{1}{\varepsilon-1}} dq \right) w_x(x, t) w(x, t)^{\frac{\varepsilon}{1-\varepsilon}} \right], \end{aligned} \quad (3.4)$$

which demonstrates that a shock in the undeformed w -system will lead to $u_{xx} \rightarrow \infty$, as it directly depends on w_x . On the other hand u_x only depends on w .

A closer inspection of the transformation (3.2) explains how a shock is converted into a peak by means of the \mathcal{PT} -deformation. Given the form of a shock profile for real $w(x, t)$, as for instance depicted in figure 1 panel (a), we first need to convert the multi-valued profile into a single valued function, which is achieved by parameterising the profile by the arc length s . From (3.2) we obtain

$$\tilde{u}(s, t) := iu(x, t)^{\frac{\varepsilon}{\varepsilon-1}} = (\varepsilon - 1)^{-1} \varepsilon^{\frac{\varepsilon-2}{\varepsilon-1}} \int^s w(q, t)^{\frac{1}{\varepsilon-1}} \frac{dq}{d\tilde{s}}, \quad (3.5)$$

with arc length element $d\tilde{s} = \sqrt{dw^2 + dx^2}$. We compute $\tilde{u}(s, t)$ for $\varepsilon = 3$, where we take the positive square root for $s < s_3$ and the negative one for $s > s_3$. When transforming back from $s \rightarrow x$ this function becomes multi-valued crossing itself as depicted in figure 1 panel (b) for a time $t_1 > t_s$.

This selection of the branches will produce a peaked function. In general the choice of the different branches is naturally governed by the appropriate boundary conditions matching the initial profile. Note that we can eliminate the part $s_1 \rightarrow s_2 \rightarrow s_3 \rightarrow s_4$ without destroying the consistency of the model and thus convert a solution from a multivalued one into a single valued peaked function. It follows by (2.11) that the conserved quantity I_κ with $\kappa = (\varepsilon - 1)^{-1}$ is unaffected by this change and remains preserved, since for that choice $\int_{-\infty}^{\infty} = \int_{-\infty}^{s_1} + \int_{s_4}^{\infty}$. However, for different values of κ the I_κ no longer constitute

charges for the peaked solution. This argument is similar to the standard introduction of a shock front, the position of which is usually chosen in such a way that I_1 is preserved. In principle this could be implemented for the undeformed system. It is clear that changing from $u(x, t)$ to $\tilde{u}(s, t)$ will not alter the argument very much, apart from introducing yet more possible branches. The peaked solutions are to be understood in the weak sense, such that a rigorous treatment requires the use of test functions.

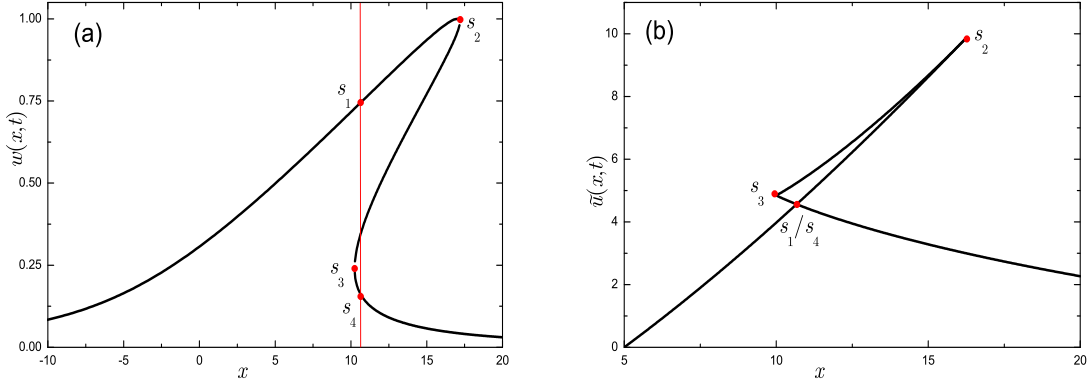


Figure 1: (a) A multi-valued self-avoiding shock wave $w(x, t_1)$. (b) Transformed multi-valued self-crossing shock wave $\tilde{u}(x, t_1)$ for $\varepsilon = 3$.

We have argued above that peaked solutions are the most common ones appearing in the deformed equations. However, under some special circumstances, that means particular initial profiles, we may also encounter shocks in the deformed system. We observe from (3.3) that $u_x \rightarrow \infty$ whenever $\int^x w(q, t)^{\frac{1}{\varepsilon-1}} dq = 0$ for $\varepsilon > 0$. In turn this means by (3.2) that $u \rightarrow 0$. Indeed one may construct such type of solutions, as we will demonstrate below.

4. Jump formation from complex shocks

So far we have focused on real solutions $w(x, t)$ for the inviscid Burgers equation. However, if we wish to consider a real transformed solution $u(x, t)$ in the case for ε not being an odd integer then in the light of (2.1) we are forced to consider also complex initial conditions. In fact, the complex inviscid Burgers equation has appeared before in the literature in several different contexts, see for example [31], [32] or [33] for applications to geostrophic flows or large N matrix models, respectively.

The method of characteristics can readily be adapted to this case. Exactly like in the real scenario, the solution is given by $w(x, t) = w_0(x_0(x, t))$, where $x_0(x, t)$ is found by inverting (2.6). Notice that in general $x_0(x, t) \in \mathbb{C}$ even for real (x, t) , so that the solution is defined by analytically continuing the initial condition to complex values of the argument.

In [34] it has been revealed that the shocks in inviscid Burgers equation are due to the presence of square root singularities of $w(x, t)$ in the complex x plane. The position of

the singularities at time t can be found by first determining x_0 by means of (2.7), and subsequently computing $x = x_0 - f(w_0(x_0))/\frac{df(w_0(x_0))}{dx_0}$.

For $t = 0$ all such singularities are located at complex infinity. Considering the solutions as functions of real x and t , with t being the parameter governing the flow, the singularities move in the complex x -plane, exhibiting a shock whenever they reach the real axis. From this discussion follows that in order to find all the possible shock times we need to impose two conditions on x_0 :

$$\operatorname{Im} \left[\frac{df(w_0(x_0))}{dx_0} \right] = 0 \quad \text{and} \quad \operatorname{Im} \left[x_0 - f(w_0(x_0))/\frac{df(w_0(x_0))}{dx_0} \right] = 0. \quad (4.1)$$

There is a crucial difference between the real and the complex case. When $w_0, f(w_0) \in \mathbb{R}$, every $x_0 \in \mathbb{R}$ solves the second equation in (4.1) and we encounter a shock for all times in some interval $[t_s, \infty)$. The reason for this is that in the real case the singularities reach the real axis in complex conjugate pairs and thereafter, i.e. for $t > t_s$, never leave it. In contrast, in the complex case the solutions of the second equation in (4.1) are in general isolated points in the complex plane, so that a gradient catastrophe will be an isolated event in time. The mechanism responsible for the jump is the application of a matching condition between the initial boundary condition and the ones for the evolved solution. Usually the boundary conditions are taken to be physical, that is asymptotically vanishing. Unlike as in the real case, one can no longer stitch the two asymptotic solutions $w_{1/2} \rightarrow \pm\infty$ together in a continuous manner, but instead one is forced to introduce a jump.

We shall now support and illustrate our general findings with some numerical studies.

5. Numerical case studies

5.1 Real w and real u

The $\varepsilon = 3$ deformation with $f(w) = w$ is the simplest example allowing for real solutions for the undeformed as well as for the deformed equation. In order to be able to compare directly with the results in [23] we consider here the same initial profile of the form of a Cauchy distribution $u_0 = (1 + x^2)^{-1}$, such that by (2.5) the corresponding initial profile in the undeformed equation results to $w_0 = -12x^2/(1 + x^2)^5$. According to (2.9), the gradient catastrophe occurs therefore when

$$t_{\text{gc}}^w(x_0) = \frac{(1 + x_0^2)^6}{24x_0(4x_0^3 - 1)}. \quad (5.1)$$

This function has two distinct minima, which we identify both as shock/peak times

$$\begin{aligned} x_{0,1}^{\min} &= \frac{1}{6\sqrt{2}}\sqrt{23 - \sqrt{385}} \approx 0.216621, & t_{s,1}^w &= \frac{(95 - \sqrt{385})^6}{2^{21}3^{10}(5\sqrt{11} - 2\sqrt{35})} \approx 0.311791, \\ x_{0,2}^{\min} &= \frac{-1}{6\sqrt{2}}\sqrt{23 + \sqrt{385}} \approx -0.769392, & t_{s,2}^w &= \frac{(95 + \sqrt{385})^6(5 + \sqrt{385})^{-1}}{2^{18}3^{10}\sqrt{2(23 + \sqrt{385})}} \approx 0.644466. \end{aligned} \quad (5.2)$$

In a system with shocks the second time is usually not easy to realise numerically, but for the deformed systems these times correspond to peaks and are directly accessible in numerical simulations. The numerical values for the times agree with those provided in [23]. In addition we compute from (2.8) the corresponding positions of the shocks/peaks as

$$x_{s,1}^w = \frac{3(19\sqrt{385} - 365)}{64(5\sqrt{11} - 2\sqrt{35})} \approx 0.0770263, \quad x_{s,2}^w = -\frac{3\sqrt{\frac{1}{2}(23 + \sqrt{385})}}{16} \approx -1.21712. \quad (5.3)$$

Figure 2 panel (a) exhibits how a shock develops in the undeformed system at the time $t_{s,1}^w$ and position $x_{s,1}^w$ as predicted by (5.2) and (5.3), respectively. In panel (b) we observe that a peak develops at the same times and positions $t_{p,1}^u = t_{s,1}^w$, $x_{s,1}^u = x_{s,1}^w$ and also at $t_{p,2}^u = t_{s,2}^w$, $x_{s,2}^u = x_{s,2}^w$. For the deformed system the numerical integration over the discontinuities does not pose any major obstacle and the event of the second peak can be simulated simply by integrating until that time.

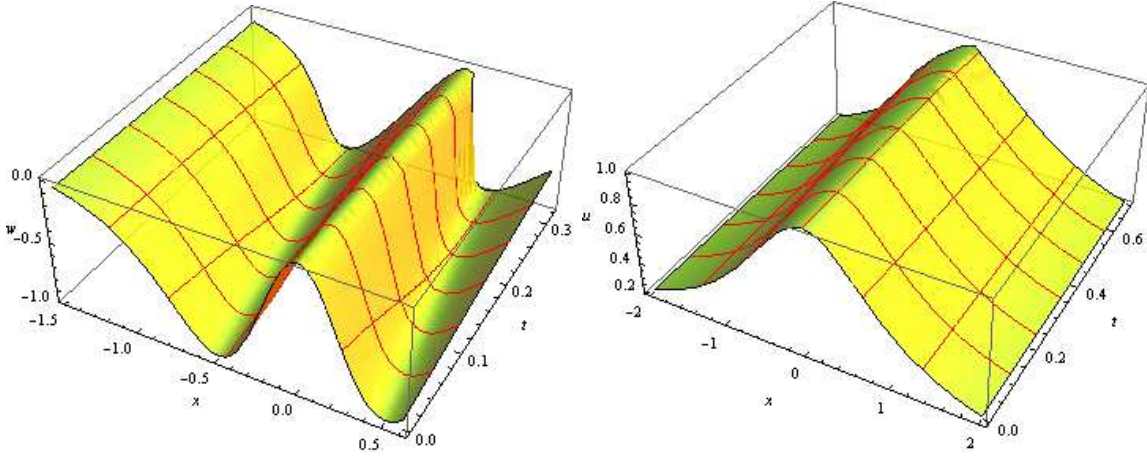


Figure 2: (a) Solution of the inviscid Burgers equation for transformed Cauchy distribution initial profile. (b) Solutions of the $\varepsilon = 3$ -deformation with Cauchy distribution initial profile.

In contrast, for the undeformed system this is not possible in such a straightforward manner because after the first shock time the function $w(x, t)$ becomes multi-valued, such that the standard procedure becomes meaningless. In principle this problem can be overcome by introducing a shock front and the preservation of some conserved quantities as argued above. For a detailed survey on these techniques see e.g. [35]. Here this is not needed and instead we can use the fact that our undeformed system is implicitly solved by $w = w_0(x - wt)$ which we can solve numerically for $w(x, t)$. Subsequently $u(x, t)$ is computed from (3.2).

The results of this computation are depicted in figure 3, which shows that the second shock time $t_{s,2}$ and position $x_{s,2}$ are approached at their predicted values (5.2) and (5.3), respectively. These positions in space and time coincide with those of the second peak in the deformed system. In panel (b) we observe that the effect on the smoothness of the curve is much less pronounced for the second "peak". In this case it is hardly visible due to fact that it is not located on the crest of the wave.

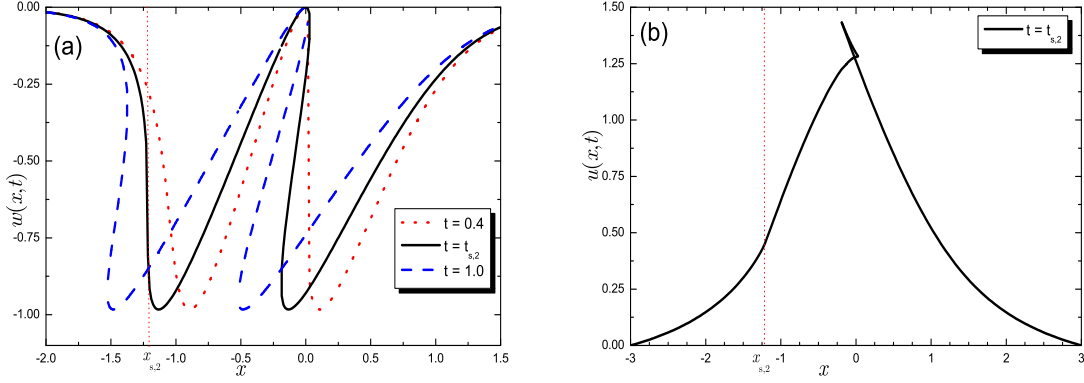


Figure 3: (a) Solution of the inviscid Burgers equation at times before and after the second shock formation with $t = 0.4$ dotted (red), the second shock time $t = t_{s,2}$ solid (black) and $t = 1.0$ dashed (blue) for transformed Cauchy distribution initial profile. (b) Solution of the $\varepsilon = 3$ -deformation of the inviscid Burgers equation at the second shock time $t = t_{s,2}$ for transformed Cauchy distribution initial profile.

Let us now present an example for the formation of a shock rather than a peak. For the deformed system we take as initial profile $u_0 = x/(1+x^2)$, such that the initial profile of undeformed equation results to $w_0 = -3x(1-x^2)^2/(1+x^2)^5$. According to (2.8) this system develops a shock at time $t_s^w = 1/3$ at position $x_s^w = 0$. For the undeformed system these findings are clearly confirmed by our numerical results depicted in figure 4 panel (a). Notice in panel (b) that when the solution evolves beyond the shock time two more shocks, in the sense that $u_x \rightarrow \infty$, develop when u becomes zero. This behaviour is forced by the relation between w and u , (2.2), since w is finite.

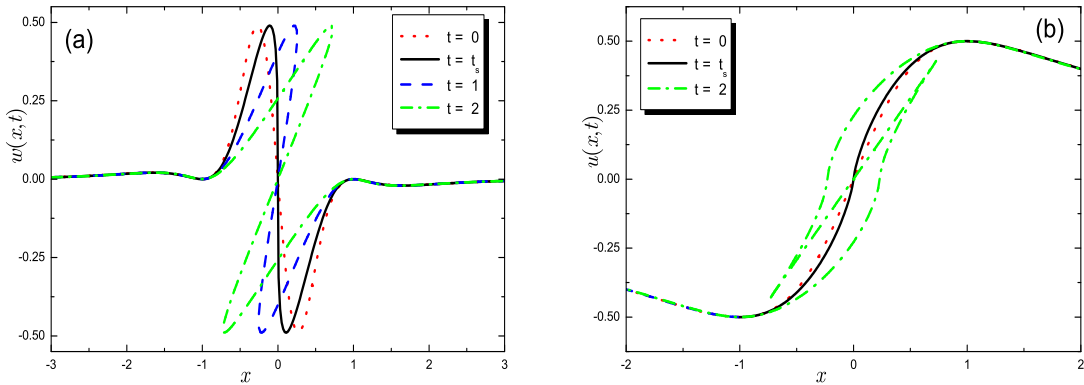


Figure 4: (a) Shock wave formation at $w = 0$ for the inviscid Burgers equation at times $t = 0$ dotted (red), the shock time $t_s = 1/3$ solid (black), $t = 1$ dashed (blue) and $t = 2$ dashdotted (green) for the transformed initial profile $x/(1+x^2)$. (b) Solution of the $\varepsilon = 3$ -deformation of the inviscid Burgers equation at $u = 0$.

5.2 Real w and complex u

The $\varepsilon = 2$ deformation with $f(w) = w$ is the easiest case to investigate the scenario for which $w \in \mathbb{R}$ and $u \notin \mathbb{R}$. We compute initially the time and position of the shock and peaks in the undeformed system (2.1), respectively.

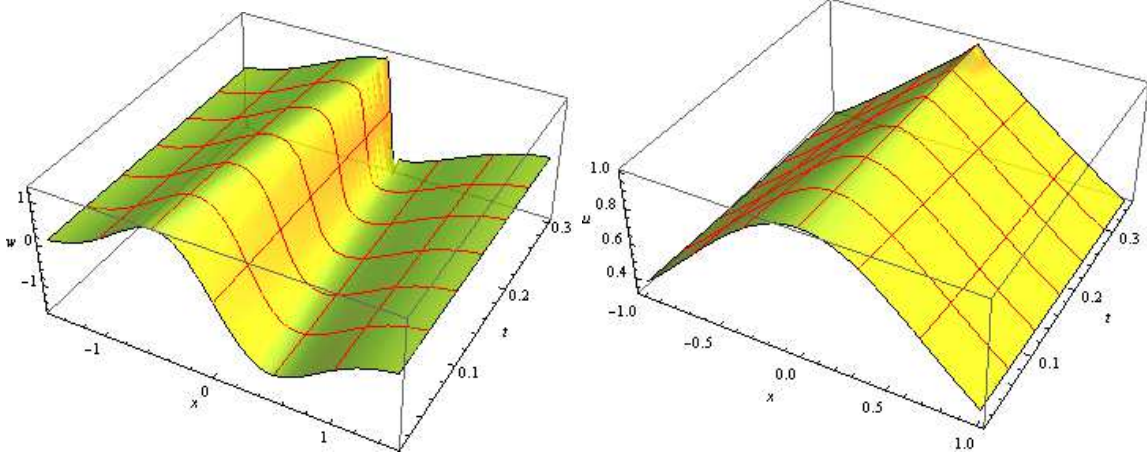


Figure 5: (a) Solutions of the inviscid Burgers equation for a transformed Gaussian initial profile. (b) Solution of the $\varepsilon = 2$ -deformation with a Gaussian initial profile in the $\exp(i\pi/4)$ -direction.

We take the initial profile to be of Gaussian form $u_0 = e^{-x^2 - i\frac{\pi}{4}}$ leading to $w_0 = -4xe^{-2x^2}$ with the help of the transformation (2.5). As argued above, to take the phase in u_0 is one possibility to guarantee real shock times. The time for the gradient catastrophe computed from (2.9) is $t_{\text{gc}}^w = e^{-x_0^2}/(4 - 16x^2)$, which becomes minimal for $x_0^{\min} = 0$. The resulting shock/peak time and position are therefore $t_s^w = t_s^u = 1/4$ and $x_s^w = x_s^u = 0$, respectively.

Figure 5 panel (a) clearly shows how a shock develops in the undeformed system at the predicted shock time t_s and position x_s . Panel (b) exhibits that in the deformed system this shock is converted into a peak occurring at the same time and position. In general this wave travels in the complex u -plane, but here we have only plotted here the $\exp(i\pi/4)$ -direction for which $u(x, t)$ becomes real. We also note that the peak becomes more pronounced as the wave evolves beyond its time of formation.

5.3 Complex w and complex u

Here we will consider the deformation with $\varepsilon = 3/2$. As discussed in section 4, we now require a complex solution for the undeformed equation in order to generate shock waves. We select a simple initial condition which vanishes asymptotically

$$w_0(x) = w(x, 0) = \frac{e^{\frac{i\pi}{4}}}{x^2 + 1}. \quad (5.4)$$

and in addition allows to solve the well known implicit relation $w = w_0(x - wt)$. The transformation (2.2) then guarantees that we have real initial conditions for the deformed

equation

$$u_0(x) = \left[\frac{4}{3} \int_{-\infty}^x \frac{1}{(y^2 + 1)^2} dy \right]^{1/3}, \quad (5.5)$$

with boundary conditions

$$\lim_{x \rightarrow -\infty} u_0(x) = 0, \quad \lim_{x \rightarrow +\infty} u_0(x) =: k \approx 1.2794, \quad \text{and} \quad \lim_{x \rightarrow \pm\infty} \partial_x u_0(x) = 0. \quad (5.6)$$

We demand that these boundary conditions are preserved for $t > 0$.

Given w_0 , we compute the shock time as outlined in section 4. The conditions (4.1) have two solutions: $z_{0,1} \approx 0.164903 - 0.553299i$ and $z_{0,2} = -z_{0,1}$, and, correspondingly, we find two shock times: $t_{s,1} \approx 0.4791 > 0$ and $t_{s,2} = -t_{s,1} < 0$. The shock occurring for positive time is located at $x_{s,1} \approx 0.494709$.

In figure 6, we plot real and imaginary part of the solution $w(x, t)$, obtained by inverting the relation $w = w_0(x - wt)$. In this example, $w(x, t)$ has three branches, of which only two are represented in the figure. The branch represented as a solid (black) line is the solution satisfying the initial condition (5.4).

We see that the two branches touch at $t = t_{s,1}$. For $t > t_{s,1}$, the left part of one branch has connected with the right part of the other, imposing a jump on the physical solution in order to preserve the asymptotic behaviour $\lim_{x \rightarrow \pm\infty} w(x, t) = 0$.

To see how this reflects on the evolution of the deformed field, we have constructed the solution $u(x, t)$ using the relation (3.2)

$$u(x, t) = \left[-\frac{4i}{3} \int_{-\infty}^x w(y, t)^2 dy \right]^{1/3}, \quad (5.7)$$

and evaluated the integral numerically. In figure 7, we represent $u(x, t)$ for a sequence of times leading to $t_{s,1}$, and we observe again that u_x is continuous, while $u_{xx}(x_{s,1}) \rightarrow \infty$ as $t \rightarrow t_{s,1}$.

After the shock time, $w(x, t)$ develops a jump. We will show that the boundary conditions (5.6) impose a jump on $u(x, t)$ as well. In order to see this we will try to match the following expressions:

$$\hat{u}(x, t) = \left(-\frac{4i}{3} \int_{-\infty}^x w^{(1)}(y, t)^2 dy \right)^{\frac{1}{3}}; \quad (5.8)$$

$$\tilde{u}(x, t) = \left(k^3 - \frac{4i}{3} \int_{+\infty}^x w^{(2)}(y, t)^2 dy \right)^{\frac{1}{3}}, \quad (5.9)$$

where the two branches $w^{(1,2)}(x, t)$ are defined by: $w^{(1)}(-\infty, t) = 0 = w^{(2)}(+\infty, t)$ for $t > t_{s,1}$. By construction, $\hat{u}(x, t)$ satisfies the left boundary condition in (5.6), while $\tilde{u}(x, t)$ satisfies the condition on the right.

In figure 8 we show $\hat{u}(x, t)$ and $\tilde{u}(x, t)$ for $t = 1$. We notice that, contrary to the real case treated in section 3, we can not find an x_* such that $\hat{u}(x_*, t) = \tilde{u}(x_*, t)$. This can be understood because the former condition now splits into two real equations, while we have only one real parameter x_* to tune. The consequence is that a continuous solution for $u(x, t)$ does not exist beyond $t_{s,1}$.

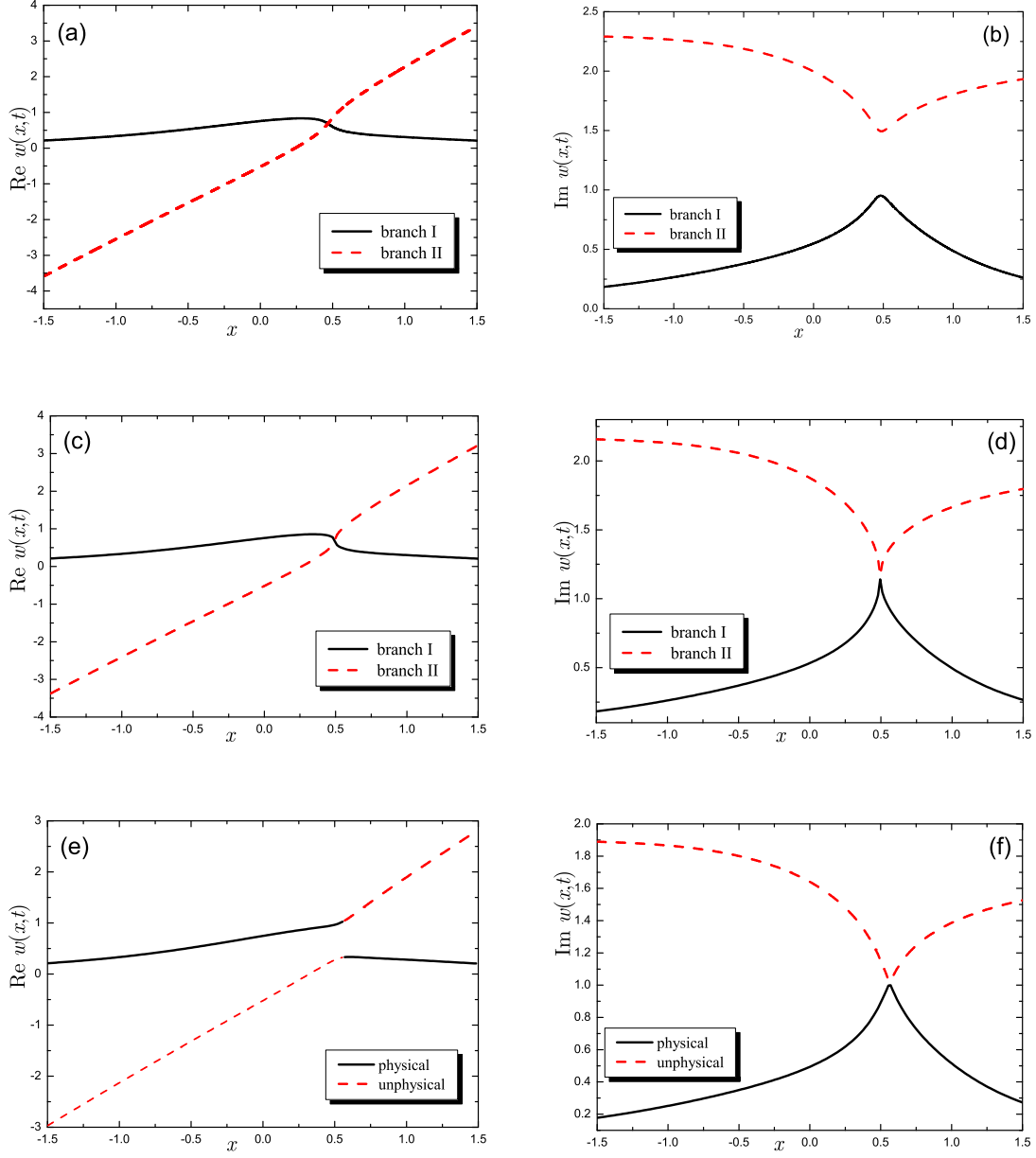


Figure 6: (a), (b) Real and imaginary part of the solution of the inviscid Burgers equation with complex initial condition (5.4) solid (black) and a second, unphysical branch dashed (red) at time $t = 0.45 < t_{s,1}$. (c), (d) The two branches touching at the shock time $t = t_{s,1}$. (e), (f) The physical solution with vanishing asymptotic boundary conditions exhibits a jump discontinuity at $t = 0.55 > t_{s,1}$.

5.4 Deformations with odd ε and $f(w) = w$

We will now study how the systems behave as a function of increasing values of the deformation parameter ε . We keep the initial profile in the deformed system to be a Cauchy

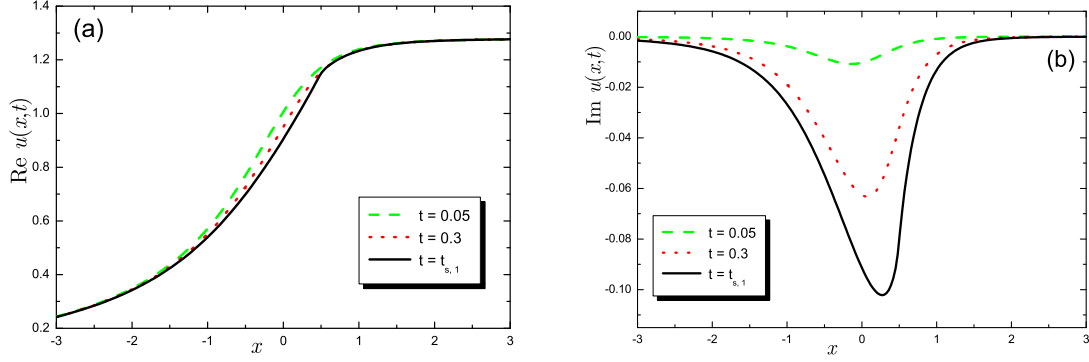


Figure 7: Real and imaginary parts of the solution of the deformed Burgers equation with $\varepsilon = 3/2$ and initial condition (5.5) for $t = 0.05$ dashed (green), $t = 0.3$ dotted (red) and at the shock time $t = t_{s,1}$ solid (black).

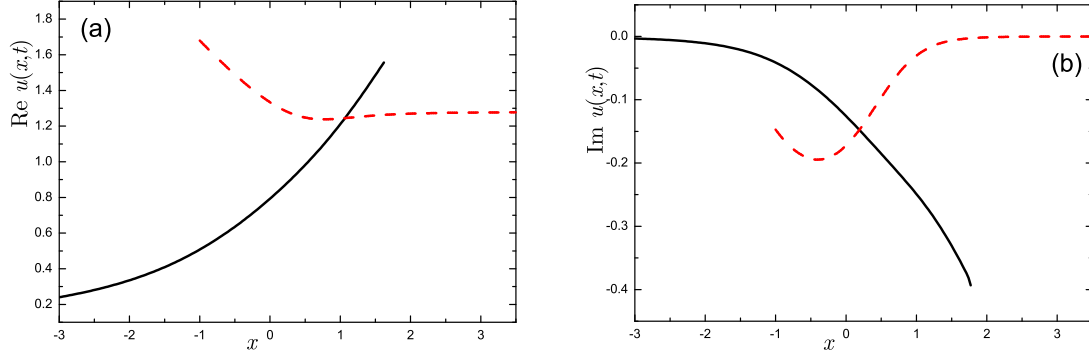


Figure 8: Real and imaginary parts of the two functions $\hat{u}(x, t)$ solid (black) and $\tilde{u}(x, t)$ dotted (red) defined in (5.8), for $t = 1$. The condition $\text{Re } \hat{u}(x, t) = \text{Re } \tilde{u}(x, t)$ is satisfied for $x = x_1 \approx 1.0663$, and the condition $\text{Im } \hat{u}(x, t) = \text{Im } \tilde{u}(x, t)$ for $x = x_2 \approx 0.1893 \neq x_1$.

distribution $u_0 = (1 + x^2)^{-1}$, such that by (2.5) the initial profile in the undeformed equation will change. We do not report the explicit expressions for these functions here, but only the resulting shock and peak times the following table:

ε	$t_{s,1}$	$t_{s,2}$	$x_{s,1}$	$x_{s,2}$
3	0.311791	0.644466	0.0770262	-1.21712
5	0.394011	0.662872	-0.18255	1.05226
7	0.594697	0.913866	0.241058	-0.970114
9	0.997223	1.45053	-0.279227	0.919109
11	1.78617	2.50127	0.306641	-0.883621
13	3.34619	4.555	-0.327569	0.857142

In figure 9 panels (a), (b) we observe that the first shock times are reproduced in our

numerical solutions and that they occur at the predicted locations.

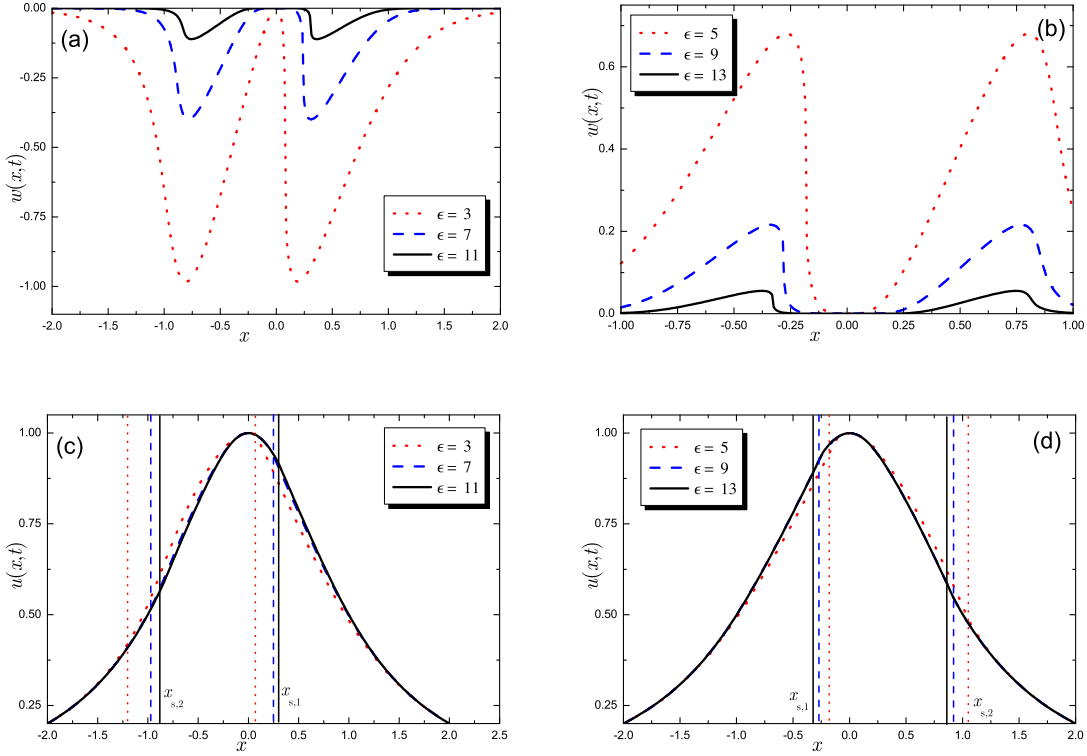


Figure 9: (a), (b) Solutions of the undeformed system at the shock time $t_{s,1}$ for various values of ϵ with transformed Cauchy distribution initial profile. (c), (d) Solution of the deformed system at the shock time $t_{s,1}$ for a Cauchy distribution initial profile.

We observe that the overall qualitative behaviour does not change with increasing values of ϵ , but the amplitudes are considerably reduced. We also note that the systems with $\epsilon = 4m - 1$ and $\epsilon = 4m + 1$ with $m \in \mathbb{N}$ break first on the right and left wave front, respectively. In the panels (c) and (d) we observe that the shocks have been smoothed out considerably and that the larger ϵ becomes the less pronounced they are. The peaks are extremely small when they occur on the tails of the waves rather than on its crest.

5.5 Multi-peak solutions

In the same way as for as for peakons an interesting question is whether it is possible to obtain multi-peaked solutions. We demonstrate here that the answer to this is affirmative. As an example we consider the equations with $f(w) = w$ and deformation parameter $\epsilon = 3$. Taking then for instance the initial profile in the deformed system to be a sum of two shifted Cauchy distributions $u_0 = [1 + (x - 1)^2]^{-1} + [1 + (x + 1)^2]^{-1}$, the initial profile of undeformed equation results to $w_0 = -96 (x^2 + 2) (x^5 + 4x^3 - 4x)^2 (x^4 + 4)^{-5}$. By means of (2.9) the

time for the gradient catastrophe is then computed to

$$t_{gc}^w(x_0) = -\frac{(x^4 + 4)^6}{384x(2x^{14} + 25x^{12} + 60x^{10} - 156x^8 - 384x^6 + 240x^4 + 192x^2 - 64)}. \quad (5.10)$$

Minimising this function we find four shock/peak times $t_{s1} = 0.221045$, $t_{s2} = 0.429609$, $t_{s3} = 0.558845$, $t_{s4} = 0.798264$ and corresponding positions $x_{s1} = 1.01299$, $x_{s2} = -2.21359$, $x_{s3} = -0.856069$, $x_{s4} = 0.116185$. All these values are accurately reproduced in figure 10. Once again the peaks emerging on the crest of the wave are well pronounced.

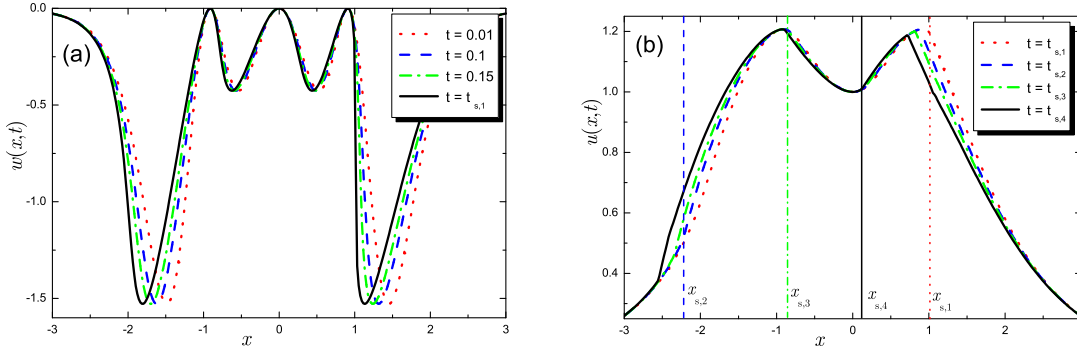


Figure 10: (a) Solutions of the inviscid Burgers equation for transformed sum of shifted Cauchy distribution initial profile at shock peak times t_{s1} dotted (red), t_{s2} dashed (blue), t_{s3} dashed (green) and t_{s4} solid (black). (b) Solutions for its $\varepsilon = 3$ -deformation at the same times and Cauchy distribution initial profile.

6. Conclusions

For large a class of nonlinear wave equations of inviscid Burgers type (2.1) we have shown that their real shock wave solutions are smoothed out in their \mathcal{PT} -symmetrically deformed counterparts into peaks. The mechanism for the peak formation was identified to be the folding of a self-avoiding multi-valued function into self-crossing multi-valued function. Under the preservation of certain conservation laws one can consistently eliminate the looping part of the self-crossing multi-valued function and thus converting it into a single valued weak solution of the deformed wave equation. In general, we found that the larger the deformation parameter ε the smoother the peaks. Our analytical arguments were facilitated by the explicit knowledge of the \mathcal{PT} -transformation from one system to the other.

We also showed that shocks in the complex solutions for the undeformed equations will lead to discontinuities in the solutions for the deformed equations.

It would be of great interest to construct more explicit maps for different types of nonlinear wave equations to their \mathcal{PT} -symmetrically deformed counterparts, such as for instance for the KdV equation.

As a practical application one may potentially use these observation in numerical investigations of nonlinear wave equations with shock wave formations. In general those equations are difficult to handle, even numerically, but one can exploit our observations by first solving the deformed equations, which are simpler to deal with as they just exhibit peaks and then transform those solutions to the undeformed system.

Acknowledgments: AC is supported by a City University Research Fellowship.

References

- [1] C. M. Bender and S. Boettcher, Real Spectra in Non-Hermitian Hamiltonians Having PT Symmetry, *Phys. Rev. Lett.* **80**, 5243–5246 (1998).
- [2] C. M. Bender, Making sense of non-Hermitian Hamiltonians, *Rept. Prog. Phys.* **70**, 947–1018 (2007).
- [3] A. Mostafazadeh, Pseudo-Hermitian Representation of Quantum Mechanics, *Int. J. Geom. Meth. Mod. Phys.* **7**, 1191–1306 (2010).
- [4] P. Assis, Non-Hermitian Hamiltonians in Field Theory, VDM Verlag Dr. Müller, Saarbrücken (2010).
- [5] A. Nanayakkara, Classical trajectories of 1D complex non-Hermitian Hamiltonian systems, *J. Phys.* **A37**, 4321–4334 (2004).
- [6] C. M. Bender, D. D. Holm, and D. W. Hook, Complex Trajectories of a Simple Pendulum, *J. Phys.* **A40**, F81–F90 (2007).
- [7] C. M. Bender, D. C. Brody, and D. W. Hook, Quantum effects in classical systems having complex energy, *J. Phys.* **A41**, 352003 (2008).
- [8] C. M. Bender, D. W. Hook, P. N. Meisinger, and Q.-h. Wang, Complex Correspondence Principle, *Phys. Rev. Lett.* **104**, 061601 (2010).
- [9] C. M. Bender, D. W. Hook, and K. S. Kooner, Classical Particle in a Complex Elliptic Potential, *J. Phys.* **A43**, 165201 (2010).
- [10] C. M. Bender and T. Arpornthip, Conduction bands in classical periodic potentials, *Pramana J. Phys.* **73**, 259–268 (2009).
- [11] C. M. Bender, D. D. Holm, and D. W. Hook, Complexified Dynamical Systems, *J. Phys.* **A40**, F793–F804 (2007).
- [12] C. M. Bender, J. Feinberg, D. W. Hook, and D. J. Weir, Chaotic systems in complex phase space, *Pramana J. Phys.* **73**, 453–470 (2009).
- [13] A. Fring, A note on the integrability of non-Hermitian extensions of Calogero-Moser-Sutherland models, *Mod. Phys. Lett.* **21**, 691–699 (2006).
- [14] A. Fring and M. Znojil, \mathcal{PT} -Symmetric deformations of Calogero models, *J. Phys.* **A40**, 194010(17) (2008).
- [15] P. E. G. Assis and A. Fring, From real fields to complex Calogero particles, *J. Phys.* **A42**, 425206(14) (2009).
- [16] A. Fring and M. Smith, Antilinear deformations of Coxeter groups, an application to Calogero models, *J. Phys.* **A43**, 325201(28) (2010).

- [17] A. Fring and M. Smith, Non-Hermitian multi-particle systems from complex root spaces, arXiv 1108.1719 .
- [18] P. K. Ghosh, On the construction of pseudo-hermitian quantum system with a pre-determined metric in the Hilbert space, *J. Phys.* **A43**, 125203 (2010).
- [19] P. K. Ghosh, Deconstructing non-Dirac Hermitian supersymmetric quantum systems, *J. Phys.* **A44**, 215307 (2011).
- [20] C. M. Bender, D. C. Brody, J. Chen, and E. Furlan, \mathcal{PT} -symmetric extension of the Korteweg-de Vries equation, *J. Phys.* **A40**, F153–F160 (2007).
- [21] A. Fring, \mathcal{PT} -Symmetric deformations of the Korteweg-de Vries equation, *J. Phys.* **A40**, 4215–4224 (2007).
- [22] B. Bagchi and A. Fring, \mathcal{PT} -symmetric extensions of the supersymmetric Korteweg-De Vries equation, *J. Phys.* **A41**, 392004(9) (2008).
- [23] C. M. Bender and J. Feinberg, Does the complex deformation of the Riemann equation exhibit shocks?, *J. Phys.* **A41**, 244004 (2008).
- [24] T. L. Curtright and D. B. Fairlie, Euler Incognito, *J. Phys.* **A41**, 244009 (2008).
- [25] C. M. Bender, F. Cooper, A. Khare, B. Mihaila, and A. Saxena, Compactons in \mathcal{PT} -symmetric generalized Korteweg-de Vries Equations, *Pramana J. Phys.* **73**, 375–385 (2009).
- [26] P. E. G. Assis and A. Fring, Compactons versus Solitons, *Pramana J. Phys.* **74**, 857–865 (2010).
- [27] A. Cavaglia, A. Fring, and B. Bagchi, PT-symmetry breaking in complex nonlinear wave equations and their deformations, *J. Phys.* **A44**, 325201 (2011).
- [28] R. Camassa and D. Holm, An integrable shallow water equation with peaked solitons, *Phys. Rev. Lett.* **71**, 1661–1664 (1993).
- [29] E. Wigner, Normal form of antiunitary operators, *J. Math. Phys.* **1**, 409–413 (1960).
- [30] R. Gopakumar and D. J. Gross, Mastering the master field, *Nucl. Phys.* **B451**, 379–415 (1995).
- [31] G. R. Baker, X. Li, and A. C. Morlet, Analytic structure of two 1D-transport equations with nonlocal fluxes, *Physica D: Nonlinear Phenomena* **91**, 349–375 (1996).
- [32] D. Chae, A. Crdoba, D. Crdoba, and M. A. Fontelos, Finite time singularities in a 1D model of the quasi-geostrophic equation, *Advances in Mathematics* **194**, 203–223 (2005).
- [33] A. Matytsin, On the large N limit of the Itzykson-Zuber integral, *Nucl. Phys.* **B411**, 805–820 (1994).
- [34] D. Bessis and J. D. Fournier, Pole condensation and the Riemann surface associated with a shock in Burgers’ equation, *J. Physique Lett.* **45**, 833–841 (1984).
- [35] R. J. LeVeque, Numerical Methods for Conservation Laws, Lectures in Mathematics ETH Zurich, Birkhäuser (1992).